An investigation on the effect of different multi-step heat treatments on the microstructure, texture and mechanical properties of the DED-produced Ti-6Al-4V alloy

Materials Characterization 189 (2022) 111958

Contents lists available at ScienceDirect

Materials Characterization

journal homepage: www.elsevier.com/locate/matchar

An investigation on the effect of different multi-step heat treatments on the microstructure, texture and mechanical properties of the DED-produced Ti-6Al-4V alloy

Alessandro Carrozza [a,b,*], Alberta Aversa [b,c], Federico Mazzucato [d], Emilio Bassini [b,c], Diego Manfredi [b,c], Sara Biamino [b,c], Anna Valente [d], Paolo Fino [b,c]

[a] University of Bergamo, Department of Engineering and Applied Science, Viale Marconi 5, 24044 Dalmine (BG), Italy
[b] Consorzio Interuniversitario Nazionale per la Scienza e Tecnologia dei Materiali (INSTM), Via Giuseppe Giusti 9, 50121 Firenze, Italy
[c] Politecnico di Torino, Department of Applied Science and Technology, Corso Duca degli Abruzzi 24, 10129 Torino, Italy
[d] SUPSI, Institute of Systems and Technologies for Sustainable Production, Galleria 2, Manno 6928, Switzerland

ARTICLE INFO

Keywords:
Additive manufacturing
Directed energy deposition
Heat treatments
Microstructure
Texture
Electron backscatter diffraction

ABSTRACT

This work deals with the effect of different heat treatments on directed energy deposition (DED)-produced Ti-6Al-4V samples. Annealing treatments at 1050 °C followed by different cooling rates were conducted to allow a complete recrystallization of the microstructure and remove the columnar prior-β grains, thus increasing the overall isotropy of the material. An agine treatment at 540 °C was also performed for further microstructural stabilization. The microstructures, textures and mechanical properties were then assessed. Due to the heat treatments, greatly differing microstructures were achieved in an equiaxed grain morphology. However, a "grain memory" effect was detected which resulted in the grains size increasing along the height of the samples. This effect was correlated to the intrinsic prior-β grain width variation along Z on the as-printed specimens, typical of the DED technology. Electron backscatter diffraction analyses proved that the intensity of the preferential directions increased after the heat treatments, likely due to the crystallographic variant selection mechanisms taking place when the samples cool down from the annealing temperature. This effect is also influenced by the significant difference in terms of prior-β grains sizes between the heat-treated and the as-printed specimens. To sum up, a complete homogenization of the material via heat treatment above the β-transus temperature proved to be challenging. In fact, the data suggest that the intrinsic texture-related anisotropy granted by the manufacturing process is very difficult to be eliminated.

1. Introduction

Additive manufacturing (AM) processes allow the production of full 3D components from a digital file. These innovative family of technologies is well-suited for metal processing and usually relies on pre-alloyed powders as a feedstock material. Among AM techniques, Directed Energy Deposition (DED) is very promising in terms of build-up rate, maximum size of the components and possibility to repair pre-existing parts. One of the most widely DED-processed material is the Ti-6Al-4V alloy, which is well-established in the overall AM market. Its tensile properties in the as-built state are usually superior to that of the conventionally-processed material. However, the resulting ductility is quite reduced, which is a strong limiting factor in terms of applicability [1,2]. These mechanical properties result from the high amount of residual martensite (α'), which has a moderate strengthening effect coupled with a strong embrittling character [3]. The α' formation occurs due to the high cooling rates developed during the deposition process as a result of the action of the laser. A cooling rate higher than 425 °C/s is needed to obtain a completely martensitic microstructure [4]. This value is significantly lower than the typical cooling rate of a DED process, which lies around $0.5–1{\cdot}10^4$ °C/s [5,6]. Anisotropy is another issue related to DED, which is strongly connected to the columnar prior-β

* Corresponding author at: University of Bergamo, Department of Engineering and Applied Science, Viale Marconi 5, 24044 Dalmine (BG), Italy.
E-mail addresses: alessandro.carrozza@unibg.it (A. Carrozza), alberta.aversa@polito.it (A. Aversa), federico.mazzucato@supsi.ch (F. Mazzucato), emilio.bassini@polito.it (E. Bassini), diego.manfredi@polito.it (D. Manfredi), sara.biamino@polito.it (S. Biamino), anna.valente@supsi.ch (A. Valente), paolo.fino@polito.it (P. Fino).

https://doi.org/10.1016/j.matchar.2022.111958
Received 1 April 2022; Received in revised form 4 May 2022; Accepted 9 May 2022
Available online 12 May 2022

grains that grow epitaxially layer-by-layer during the fabrication process due to the intrinsic directional cooling of the system. In fact, the baseplate acts as a heatsink and the resulting grains develop parallel to the development direction. This microstructural inhomogeneity results in direction-dependent mechanical properties. For example, Carroll et al. [7] measured a significantly lower ductility along the longitudinal direction. For this orientation, the authors attributed the brittle behavior of the alloy to the more consistent damaging effect on the α phase at grain boundaries during tensile loading. Apart from the preferential orientation of the prior-β grains, microstructural texturing is also a typical feature of DED-produced Ti-6Al-4 V samples, as demonstrated by several authors [8,9]. Simonelli et al. [10] proved that the preferential orientation of the α' laths in epitaxially-grown grains is the result of the preferential texture of the high temperature β grains (parent β grains), parallel to the development direction. In fact, each prior-β grain is characterized by α' needles preferentially oriented along specific directions, since the parent β grains are characterized by preferential orientations and the β → α' transformation follows the Burgers orientation relationship, generating preferential and specific α' crystallographic variants.

The critical ductility of the DED-processed Ti-6Al-4 V alloy highlights the importance of post-processing heat treatments, which provide the potential to tailor the microstructure, hence the mechanical properties, of the material according to the desired requirements. In general, the main categories of heat treatments that a duplex titanium alloys can undergo can be classified as stress-relieving, sub-β annealing and super-β annealing, listed at progressively increasing isothermal holding temperatures. After annealing, a further agine treatment is possible with the aim, for example, to completely stabilize the β phase. If properly planned, all these heat treatments can result in α' decomposition, however only a super-β transus annealing can remove the columnar prior-β grains in favor of more homogeneously-shaped equiaxed ones. This phenomenon is the result of the complete recrystallization of the microstructure that occurs at $T > T_\beta$ ($\simeq 1000$ °C). Therefore, this type of heat treatment is the only one that can be adopted to solve the issues correlated to the presence of martensite and anisotropic grains simultaneously.

Several works are available in which a sub-β transus annealing was chosen for DED-produced Ti-6Al-4 V parts [11–14]. Moreover, some authors also investigated the effect of a post-annealing agine process [15]. For instance Klimova-Korsmik et al. [16] performed water quenching on sub-β transus annealed samples, which were subsequently aged. However, this path did not induce a significant improvement of the ductility. According to the authors' knowledge, little attention was given to super-β transus annealing heat treatments conducted on laser deposited Ti-6Al-4V samples in the current literature [12]. For instance, Sterling et al. [17] heat treated laser-deposited grade 5 Ti-6Al-4V rods at 1050 °C for 2 h with the aim of improving fatigue properties via grain growth. The resulting tensile properties were promising in terms of strength, but ductility was very limited (< 4%). The authors related this feature to the presence of defects in the samples, induced by the fabrication process.

In this work, the impact of a super-β annealing heat treatment, followed by either furnace cooling, air cooling or water quenching, and subsequent agine treatment on the microstructure of DED-produced Ti-6Al-4V samples was investigated along with their preliminary effect of the mechanical properties, assessed via hardness evaluations.

2. Materials and methods

In this work, 15x15x15 mm cubes were built using a DED system composed of a Laserdyne 430 workstation and an Optomec multi-nozzle deposition head, held in the ARM lab – DTI laboratory of SUPSI (University of Applied Sciences and Arts of Southern Switzerland). Additional information on the machine can be found elsewhere [18,19]. The feedstock material was a Ti-6Al-4V Extra Low Interstitial (ELI) powder, characterized in a previous work from the authors [20]. The process parameters deployed are reported in Table 1. The deposition was conducted in a sealed environment filled with argon in order to protect the samples from oxidation and excessive interstitial elements enrichment.

The cubic samples were heat treated, for a total of three different conditions only differing by the cooling mean adopted after annealing, as reported in Table 2. All these conditions were analyzed and compared, also taking into account the data relative to the as-built (AB) state.

The equipment used to perform all the heat treatments was selected based on the cooling rate that had to be achieved after the annealing step. All the agine treatments and the annealing of the samples in the FC condition were conducted using a Pro.Ba VF800/S high-vacuum furnace. A low cooling rate (≈ 1–2 °C/min) was achieved by letting the specimens cool to room temperature at the end of every heat treatment step performed using this equipment. This system allowed to protect the samples from interstitials enrichment due to the low internal pressure achievable (as low as 10^{-6} mbar). The specimens in the AC state were annealed in a Tav minijet HP S/N 235 low pressure furnace and subsequently nitrogen quenched using a gas pressure of 6 bar. By doing so, an average cooling rate of 10–20 °C/s was achieved. This system is characterized by an operative pressure of 10^{-2} mbar, which is rather inadequate for heat treating titanium alloys. Moreover, the nitrogen flow might induce significant embrittlement in the material. In order to overcome these issues, all the samples were wrapped in AISI 304 stainless steel bags 0.5 mm thick. The samples in the WQ condition were heat treated in a Nabertherm RHTC 80–170/15 tube furnace. Their protection from the environment was guaranteed by a steady argon flow of 1.5 l/min. After annealing, the specimens were quickly removed by the furnace and immediately dropped in a steel bucket filled with water to achieve a high cooling rate.

The concentration of interstitial elements in the samples was measured using an inert gas fusion infra-red absorption LECO 736 O/N analyzer, testing three specimens per condition.

The cubic specimens were cross-sectioned parallel to the building direction, then mounted, polished and chemically etched using a Kroll solution (93% H_2O, 5% HNO_3, 2% HF) for 10 s. General microstructural observations were performed using a Leica DM ILM optical microscope and a PhenomXL Scanning Electron Microscope (SEM). In-depth microstructural analyses were performed in order to determine the size of different features (α/α' width). These data were gathered using the software imageJ and processing more than 20 micrographs per condition, leading to more than 500 features analyzed per sample. The same software was used to estimate the average grain width using the intercept method [21]. To do so, a virtual grid of vertical and horizontal lines was superimposed to the whole cross-section of the specimens, obtained via stitching together more than 150 micrographs per sample. The lines were repeated approximately every 2 mm. A similar methodology was already deployed by other authors [22,23]. X-Ray Diffraction (XRD) analyses were conducted with the aim to identify the phases in the specimens and to estimate the relative crystallographic parameters. To do so, a PANalytical X-Pert PRO diffractometer, arranged in a Bragg Brentano configuration, was deployed, adopting a Cu K_α radiation. The instrument was set to work at 40 kV and 40 mA, using a step size of 0.013° and considering a 2θ range between 30° and 60°. The cell parameters and volume were estimated using the data collected during the XRD analyses to solve the equation obtained combining the plane-space equation of hexagonal systems and the Bragg law [24]. Further details on this methodology can be found in a previous work from the authors

Table 1
Process parameters adopted for the production of the cubic specimens.

Power (W)	Scanning speed (mm/min)	Powder feed rate (g/s)	Hatching distance (mm)	*Z*-step (μm)	Scanning strategy
300	700	0.017	0.58	100	0°/90°

Table 2
List of the heat treatments considered and relative specifications.

Heat treatment	Annealing	Cooling	Agine
Furnace cooling + aging (FC)	1050 °C for 1 h	Furnace cooled	540 °C for 4 h
Air cooling + aging (AC)	1050 °C for 1 h	Air cooled	540 °C for 4 h
Water quenching + aging (WQ)	1050 °C for 1 h	Water quenched	540 °C for 4 h

[20].

The grains features were analyzed by means of a TESCAN S9000G SEM equipped with an Electron Backscatter Diffraction (EBSD) detector. The SEM operated at 20 keV and 10 nA using a step size of 0.5–1.8 μm, depending on the magnification adopted. The samples were tilted at 70° and their analyzed area was selected at the center in order to provide increased comparability.

Vickers microhardness measurements were performed using a Leica VMHT microhardness tester, set to apply a load of 300 g for 15 s. The same grid used for the evaluation of the grain size was used in order to evaluate possible correlations between the height of the samples and their hardness, as resulted in a previous article from the authors [20].

3. Results and discussion

To assess if any type of contamination occurred during the process or the post-processing heat treatments, an analysis of the fractions of interstitial elements (O,N) in all the samples was conducted (Fig. 1). This evaluation is significantly important when dealing with titanium alloys. In fact, oxygen and nitrogen are extremely soluble, even at low temperatures, and greatly influence the mechanical properties of the alloy. In particular, their embrittling effect is well known [4,25] and it is the main reason why the concentration of these elements must be kept as low as possible. In order to consider the influence of multiple elements simultaneously, the oxygen equivalent concentration ($[O]_{EQ}$) can be calculated using the following equation [26]:

$$[O]_{EQ} = [O] + 2.77[N] + 0.1[Fe] \quad (1)$$

Yan et al. [27] suggested a value of 0.22 for this parameters, which is the threshold for a completely brittle behavior.

The AB, FC and WQ samples were poorly enriched by interstitial elements and were well below the threshold value defined before. However, the AC specimens provided a markedly higher content of interstitials with an average value of 0.581%. In this scenario, the insurgence of some sort of issues during the heat treatment appeared likely.

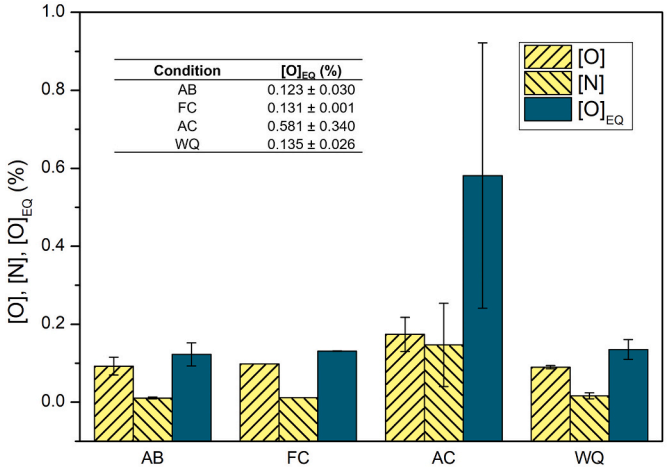

Fig. 1. [O], [N] and $[O]_{EQ}$ evaluation for all the conditions considered in this work.

Probably the method (steel bag) used to air cool the samples was probably quite inadequate, considering the extreme sensitivity of the Ti-6Al-4 V alloy to oxygen and nitrogen enrichment. This seem to be confirmed by the significant N enrichment (Fig. 1).

The analysis of the optical micrographs of all the samples confirmed that the heat treatments adopted effectively changed the prior-β grains morphology from columnar to equiaxed, due to the recrystallization process that occurred in the material when it was held at $T > T_{\beta}$. This phenomenon is clearly visible in the micrographs in Fig. 2.

Moreover, the different heat treatment conditions induced significant microstructural variations, as visible in Fig. 3. The AB specimens provided a largely α' martensitic microstructure. This feature is related to the very fast heating/cooling cycles, typical of the DED process. Conversely, the microstructural features found in the heat-treated samples were highly dependent on the cooling mean adopted.

Since most transformations occurring upon cooling from the β field are diffusional (except $\beta \rightarrow \alpha'$), the cooling mean is one of the most important heat treatment-related parameter in order to control the final microstructure of a given titanium component [3,4,28]. The samples in the FC condition underwent the slowest cooling rate, approximately 1–2 °C/min, which resulted in a completely lamellar α + β microstructure in which α colonies were easily recognizable (Fig. 3b). Moreover, thick α layers in correspondence of the prior-β grain boundaries (α_{GB}) were visible throughout the whole cross-section. Similarly, the specimens in the AC condition were characterized by fine α laths surrounded by a thin layer of β phase. Although, no clear colonies were detected, unlike in the previous case. In fact, a Widmanstätten morphology was recognized by the typical ±30°/60° angles between neighbor lamellae, typical of intermediate cooling rates (≈ 10 °C/min) [3,4]. Oppositely, the specimens in the WQ conditions provided a mainly martensitic microstructure, close to the AB case. However, a relevant number of α laths homogeneously dispersed throughout the whole sample were detected. The formation of such features via water quenching is possible, as the typical cooling rate achieved during water quenching is typically lower than 410 °C/s [29,30]. Nevertheless, the insurgence of a greater amount of α phase and its growth are more likely due to the possible decomposition of the martensite during the agine step of the heat treatment. In fact, the long duration and relatively high temperature facilitate the occurrence of diffusive phenomena, such as the $\alpha' \rightarrow \alpha + \beta$ decomposition. During this transformation, the supersaturated martensite lattice expels the β-stabilizing elements (e.g. V, Mo), thus transforming into α laths and generating a thin β layer around itself [31,32].

In order to confirm the assumptions made during the microstructural analyses of the micrographs and to investigate more in details the phases involved, the XRD patterns of all the samples were gathered and studied, as visible in Fig. 4a.

All the samples provided the peaks relative to the α/α' phases. Although, the distinction between these two phases is challenging by means of XRD patterns observation, as both are characterized by the same hexagonal structure [33,34]. The (110) peak relative to the β phase was found only in the AC and FC samples. The presence of a non-negligible amount of this phase is in good agreement with the heat treatments conducted. As a matter of facts, these two conditions underwent the lowest cooling rates which facilitated the diffusive phenomena, thus the $\beta \rightarrow \alpha + \beta$ occurred completely. Moreover, the presence of β confirms that the AC and FC conditions were both characterized by thermodynamically stable α, since no transformations during cooling allow the formation of β phase without α. Moreover, the pattern relative to the AB state was shifted towards higher 2θ values. This behavior was probably due to the residual stress accumulated in the samples during the fabrication process. This feature is nullified by the annealing phase in all the heat-treated samples. Conversely, the WQ specimens did not provide any relevant peak shift, despite being characterized by an out-of-equilibrium microstructure, which is usually associated with internal stress accumulation. This was probably due to

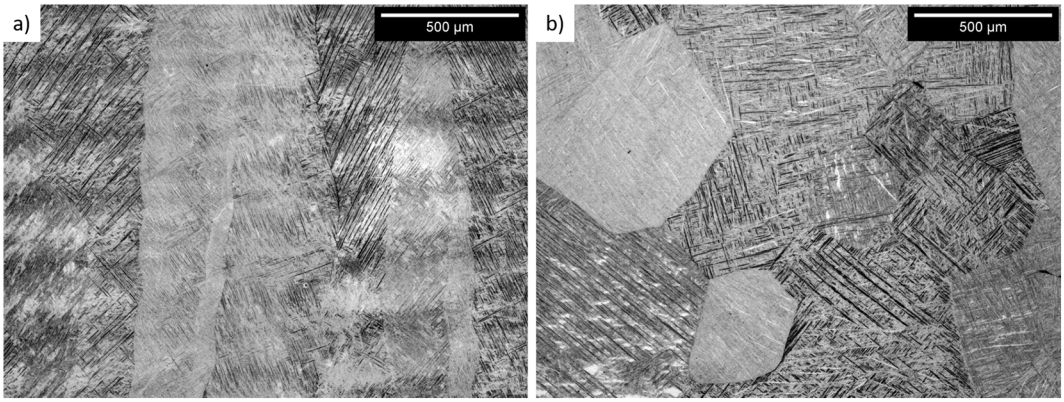

Fig. 2. Representative optical micrographs of the AB and WQ specimens, highlighting the transition from a columnar to an equiaxed grain morphology.

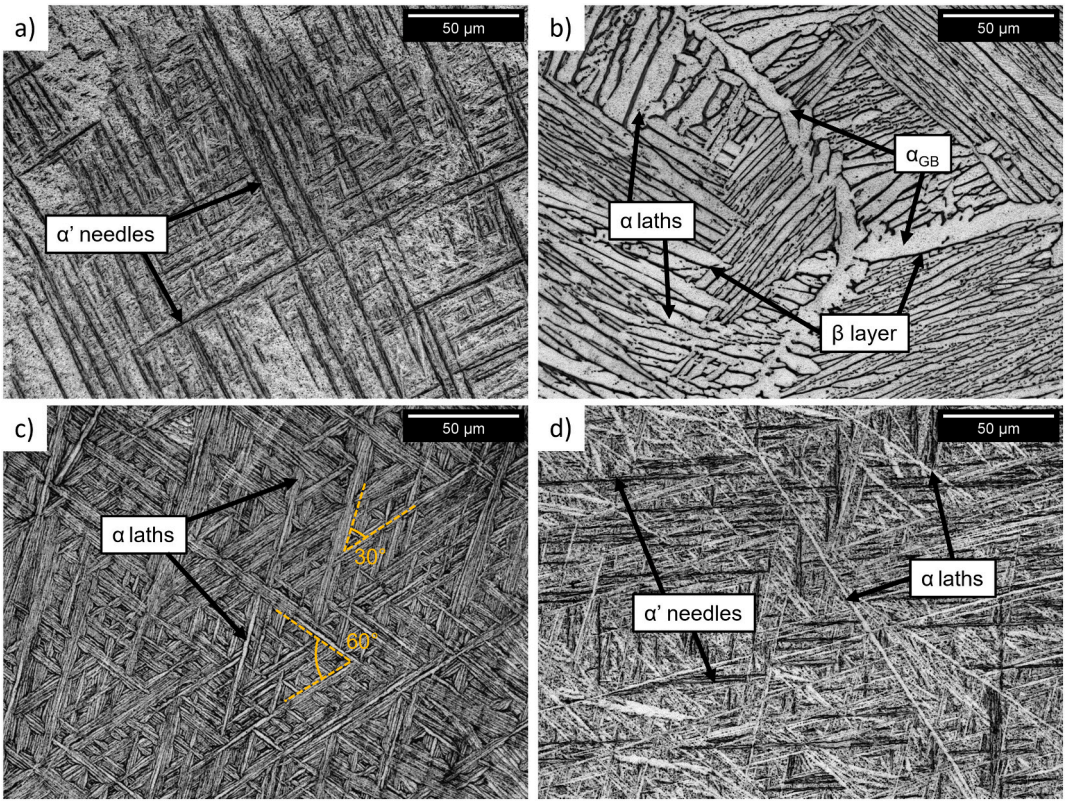

Fig. 3. Optical micrographs of the AB (a), FC (b), AC (c) and WQ (d) samples.

the agine that acted as a stress relieving treatment.

The cell parameters for the α phase were also assessed from the patterns recorded in the XRD analyses. The hexagonal (α/α') cell volume was chosen as the most suitable parameter to compare all the specimens. The outcome of this evaluation is illustrated in Fig. 4b. All the heat-treated specimens provided similar values, ranging from 34.79 to 34.83 $Å^3$. Instead, the AB samples were characterized by a smaller cell, in good agreement with the data found elsewhere for martensitic Ti-6Al-4V microstructures with considerable residual stress accumulation [35].

An in-depth microstructural investigation was also conducted to further study the microstructures of all the specimens. Since the comparison between different microstructural morphologies is challenging, two separate parameters were studied: the width of the α laths (Fig. 5a) and the width of the α' martensitic needles (Fig. 5b). The former was used to compare the heat-treated samples (FC, AC, WQ), whilst the latter was used to investigate the AB and WQ specimens only. The measurement of these microstructural features is very significant in titanium metallurgy, as the data gathered can be used to estimate the mechanical behavior of the alloy [3].

The comparison of the α width between the different heat-treated specimens (Fig. 5a) highlighted the markedly finer α phase of the AC samples, which is a typical outcome for Widmanstätten morphologies compared to lamellar colonies (FC). In fact, the former microstructure is obtained in correspondence of higher cooling rates, thus allowing a shorter time for diffusive phenomena (e.g. α growth) to occur. The α laths obtained in the WQ samples were also significantly larger. However, a direct comparison between this condition and the others is not possible. In fact, α is sparsely present in the microstructure in the WQ condition, which is mostly composed of α'. Instead, in the FC and AC scenarios, the α lamellae, and relative thin β layers, formed the whole microstructure.

By comparing the α' width for the AB and WQ conditions (Fig. 5b),

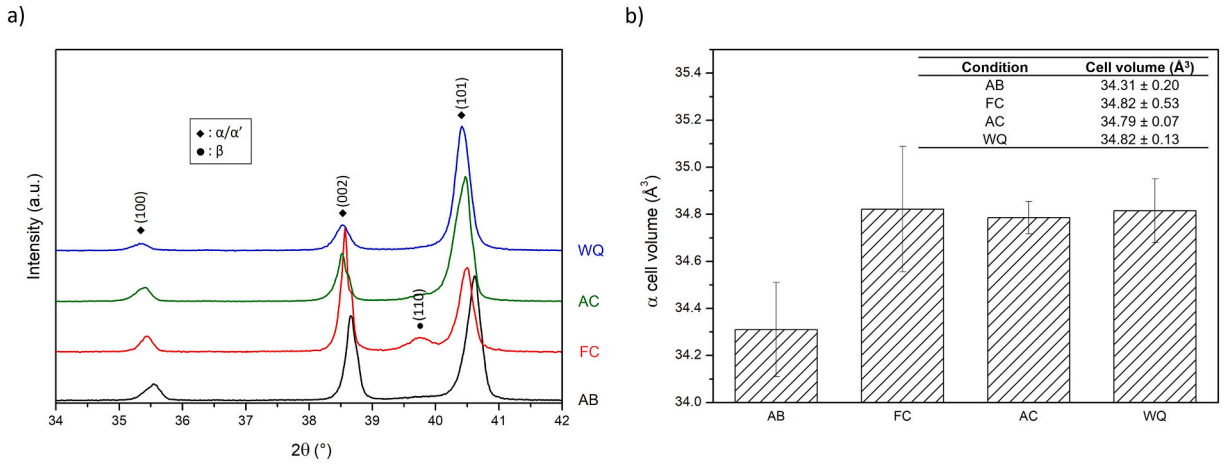

Fig. 4. XRD patterns (a) and relative cell volumes (b).

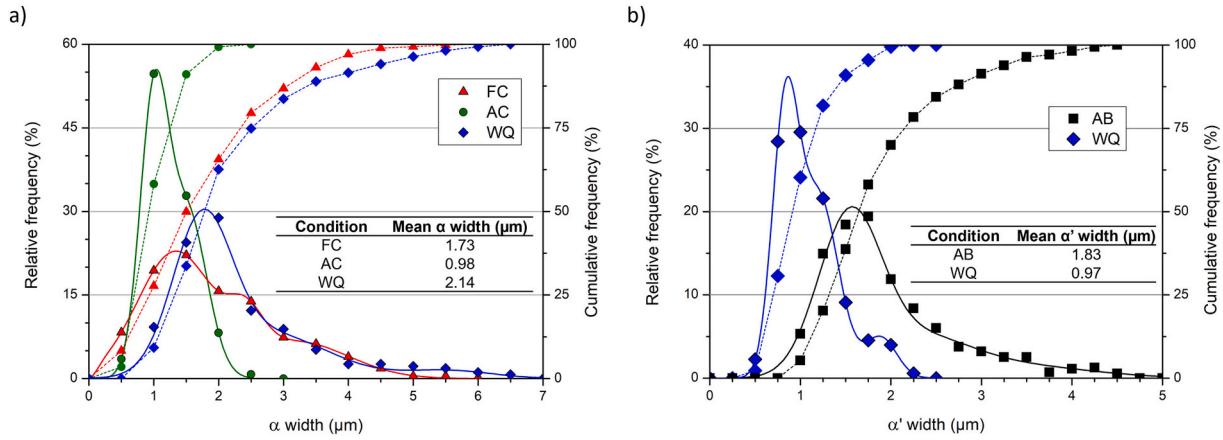

Fig. 5. Frequency (solid lines) and cumulative (dashed lines) distribution curves related to the width of the α laths in the heat-treated samples (a) and the width of the α' needles in the specimens in the AB and WQ states (b).

the latter appeared markedly finer. Since this microstructural feature is strictly dependent on the cooling rate, this result was in good agreement with the data available in the literature, which confirmed that the cooling rate is significantly lower during the quenching step ($\approx 10^2$ °C/s) than in the DED process ($\approx 10^3$–10^4 °C/s) [5,6,29,30].

As mentioned before, all the heat-treated samples provided equiaxed prior-β grains. For the sake of comparison with the AB condition, the grain width was considered, instead of the size. This approximation appeared appropriate as the aspect ratio (AR) of the equiaxed grains resulted consistently higher than 0.90. Thus, the width can be considered as representative of the size of the grain itself, when using the intercept method. The comparison of the grain widths, provided in Table 3, highlighted an overall increase of this value after the heat treatments. This was mostly related to the higher self-diffusion coefficient that characterizes the titanium β phase ($\approx 10^{-13}$ m^2/s at 1000 °C) with respect to the α phase ($\approx 10^{-15}$ m^2/s at 1000 °C) [36]. Since during the super-β transus annealing the β phase is predominant and grain enlargement is a diffusion-driven phenomenon, grain growth is expected to occur quickly.

Table 3
Average prior-β grains width.

Condition	Average prior-β grains width (mm)
AB	0.30 ± 0.06
FC	0.81 ± 0.22
AC	0.72 ± 0.18
WQ	0.82 ± 0.24

The evolution of the prior-β grains width along Z for all the samples was also investigated (Fig. 6) in order to understand whether the recrystallization of the grains was influenced by the intrinsic anisotropy of the DED-produced samples. In fact, as found in a previous work from the authors, this manufacturing process induces a grain size variation along the sample's height as a result of a difference in the cooling rate during the deposition [20]. A clear upward sloping trend was observed in all the samples. For instance, the FC specimens provided a grain width variation from 0.55 mm (proximity of the base) to 1.07 mm at a 9 mm height. This means that, even if a complete recrystallization of the material occurred via super-β transus heat treatment, a certain "grain memory" effect took place, preventing the microstructure to be completely homogenized. This phenomenon was probably due to the grain boundaries being preferential nucleation sites for newly developed grains in the β field at $T > T_\beta$ [37]. In fact, during annealing, the new β grains develop preferentially at pre-existing boundaries and then grow at the expense of the residual α phase [38].

EBSD investigations were conducted on the specimens in all conditions to further investigate the effect of the heat treatments on the texture of the α/α' phases. The β phase was not investigated due to its presence in small amounts. Different magnifications had to be set due to the significantly differing sizes provided by the microstructural features analyzed in each condition. The inverse pole figure (IPF) maps are illustrated in Fig. 7. In general, the outcome of this type of evaluations

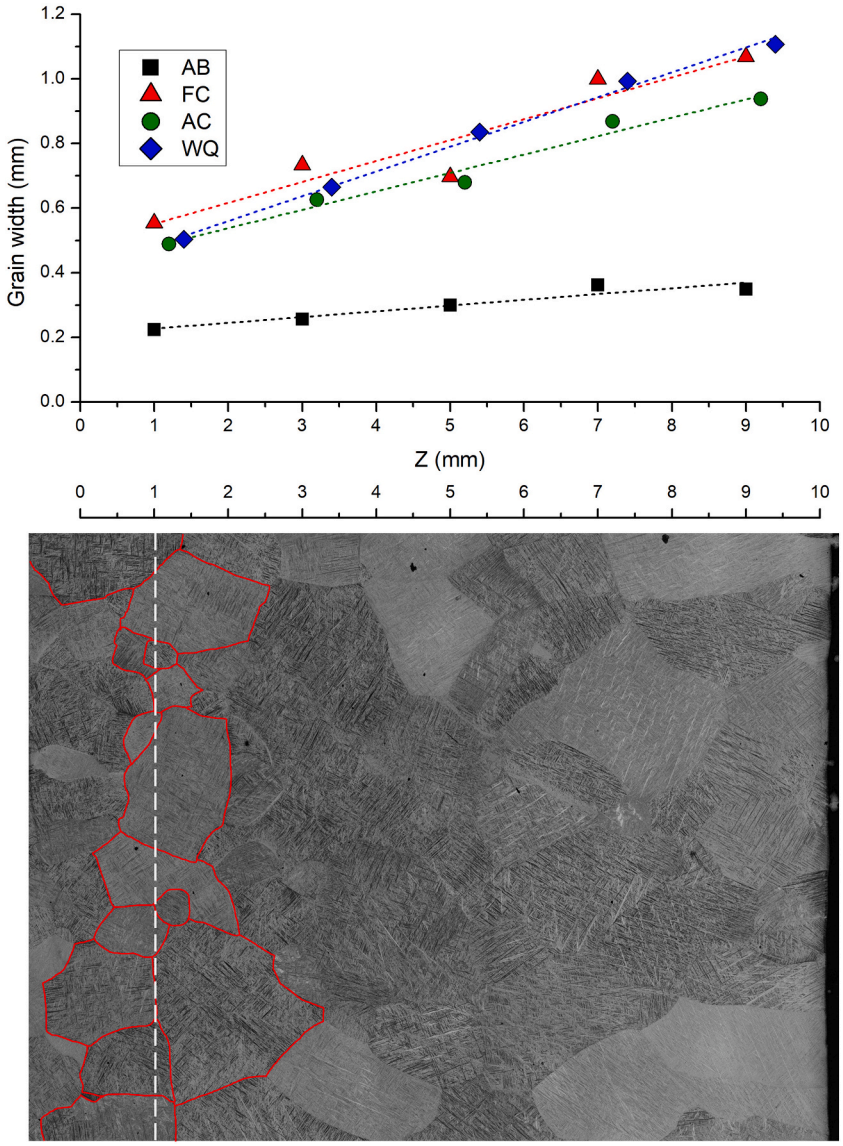

Fig. 6. Prior-β grains width trends along the height of the samples with a representative portion of a micrograph used for the evaluation of the grain size. The grains crossing the superimposed grid line are highlighted.

provides a graphical representation of the grains in a material. In this case, the images obtained highlight different microstructural features that can be linked to the micrographs in Fig. 3. In the AB and WQ IPF maps (Fig. 7a,d), the martensitic needles were clearly highlighted. Therefore, neighbor α' needles are characterized by different crystallographic orientations, even if contained the same prior-β grain. This phenomenon is due to the prior-β grains develop from parent β grains during cooling from $T > T_\beta$, following the Burgers orientation relationship. Thus, α/α' laths showing different crystallographic orientations can develop from the same parent β grain [10]. However, the variant of the high-temperature β grain still has an influence on the α' laths generated, as a limited number of preferential crystallographic orientations can be achieved in the same prior-β grain [39], as clearly visible in Fig. 7a.

To confirm the correspondence between the α' needles detected using optical microscopy and EBSD, the α' width measurements obtained by means of optical imaging (Fig. 5b) in the AB samples, were compared to the ones obtained during the EBSD analysis. The resulting trends are provided in Fig. 8. The average α' width values were 1.83 and 1.98 μm respectively. A good data fitting between the two conditions was demonstrated, confirming that the grains detected by the EBSD analysis correspond to the α' needles visible using the optical microscope. The same type of investigation was not applicable to the WQ condition due to the data divergence caused by the presence of the α laths. In the AB state, the columnar prior-β grains were still easily distinguishable and characterized by a strong internal texture, as confirmed by Cepeda-Jiménez et al. [39]. The FC samples provided big colonies, characterized by the same crystallographic and geometrical orientations. Therefore, the single lamellae were undistinguishable by means of EBSD analyses. These results are in good agreement with the microstructural analysis of the micrographs (Fig. 3b). Instead, the AC specimens (Fig. 7c) were characterized a hybrid IPF map between the other conditions: the lamellar colonies were quite visible, but their overlap due to the Widmanstätten morphology resulted in a cross-pattern of two different crystallographic orientations per colony. Similarly to the AB and WQ case, even if neighbor α laths were characterized by different variants, an overall limited number of preferential crystallographic orientations was identified inside each prior-β grain (Fig. 7c).

Similar microstructural features were highlighted in a work by Dai et al. [40], focusing on the EBSD investigation of hot-rolled Ti-6Al-4 V specimens that underwent similar heat-treatment with respect from the ones proposed in this work. The authors found the presence of lamellar

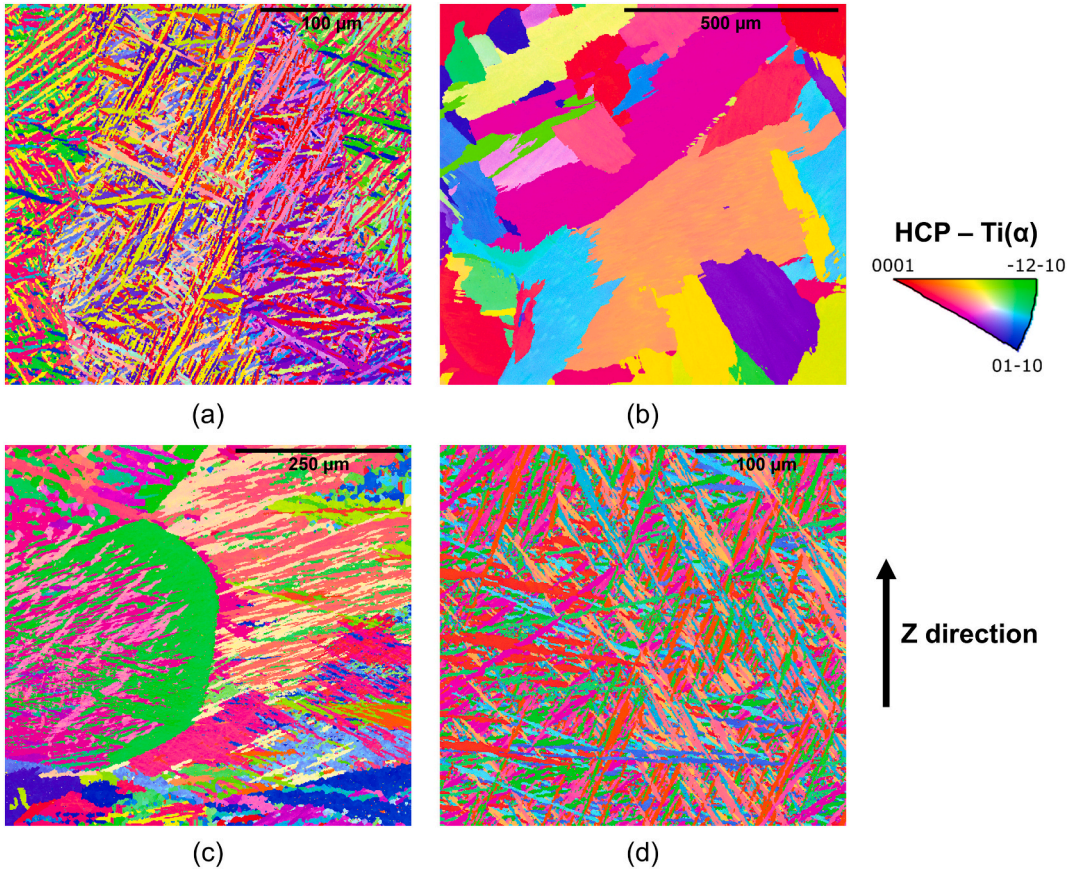

Fig. 7. Representative EBSD α/α' IPF maps along the development direction of the AB (a), FC (b), AC (c) and WQ (d) samples. The step sizes adopted were 0.5, 1.8, 1.2 and 0.5 µm, respectively.

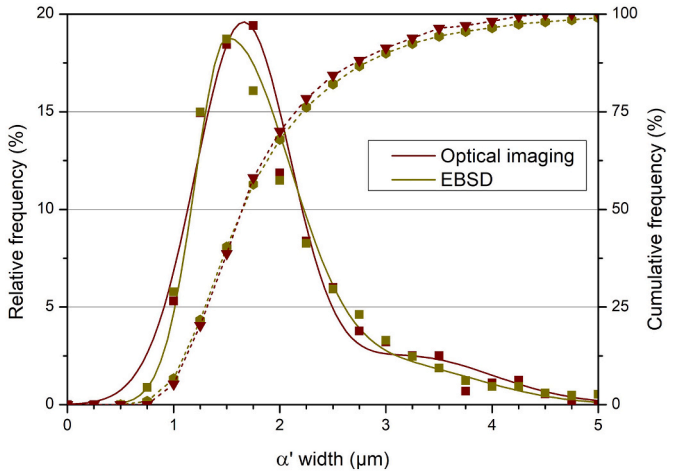

Fig. 8. Frequency (solid lines) and cumulative (dashed lines) distribution curves of the α' width measured by means of optical imaging and EBSD in the AB specimens.

colonies sharing the same crystallographic variant in the FC samples. A bast-weave lamellar structure, where parallel lamellar had the same orientations, was highlighted in the AC conditions. Moreover, martensitic laths not sharing the same variants of their neighbours were detected in the WQ samples. The most notable difference with this work lies in the size of the colonies in the FC samples, 23 µm on average by Dai et al. [40] and 58 µm in this work. This disproportion was probably due to the increased annealing time considered in this work (1 h vs. 10 min).

An in-depth textures investigation was conducted by comparing the pole figures (PF) relative to the hexagonal phase in titanium, provided in Fig. 9. All the samples were characterized by a strong preferred orientation along the ⟨0001⟩ direction. It is already established in the literature that columnar prior-β grains are characterized by a strong $\langle 0001 \rangle_\alpha$ texture, deriving from the $\langle 100 \rangle_\beta$ texture of the high temperature parent β grains, developed epitaxially during the manufacturing process [41,42]. However, this feature seems to be maintained even in the heat-treated sample, despite the recrystallization of the microstructure during the annealing.

All the specimens provided preferential crystallographic directions in the $\langle 001 \rangle_\alpha$ stereographic projections in Fig. 9. Namely, ⟨021⟩, ⟨142⟩, ⟨143⟩ and ⟨121⟩ for the AB, FC, AC and WQ conditions, respectively. The occurrence of such directions was 19.35, 44.45, 34.70 and 36.03 times random. The lower value of the AB sample can be correlated to a certain extent to the intrinsic difficulty in comparing features with greatly differing sizes. In fact, the AB specimens were characterized by significantly finer prior-β grains with respect to the heat-treated samples (Table 3), whose prior-β grains are equiaxed and closer to the size of the sample itself. This crucial feature can be overcome by reducing the magnification of the instrument. However, the features analyzed (e.g. α' needles in the WQ condition, Fig. 7d) are hardly recognizable this way. Therefore, there is an intrinsic instrumental difficulty in measuring the texture in a reliable way when the prior-β grains are significantly enlarged. This is particularly evident when dealing with the FC specimens: The relative IPF map (Fig. 7b) was obtained using a significantly lower magnification than in the AB and WQ specimens (Fig. 7a,d). Notwithstanding that, the number of features analyzed was definitely lower in the FC case. This is due to the lamellar colonies being orders of magnitude bigger than the α' laths. Moreover, there is an instrumental limit to the minimum magnification that can be used during the test. To

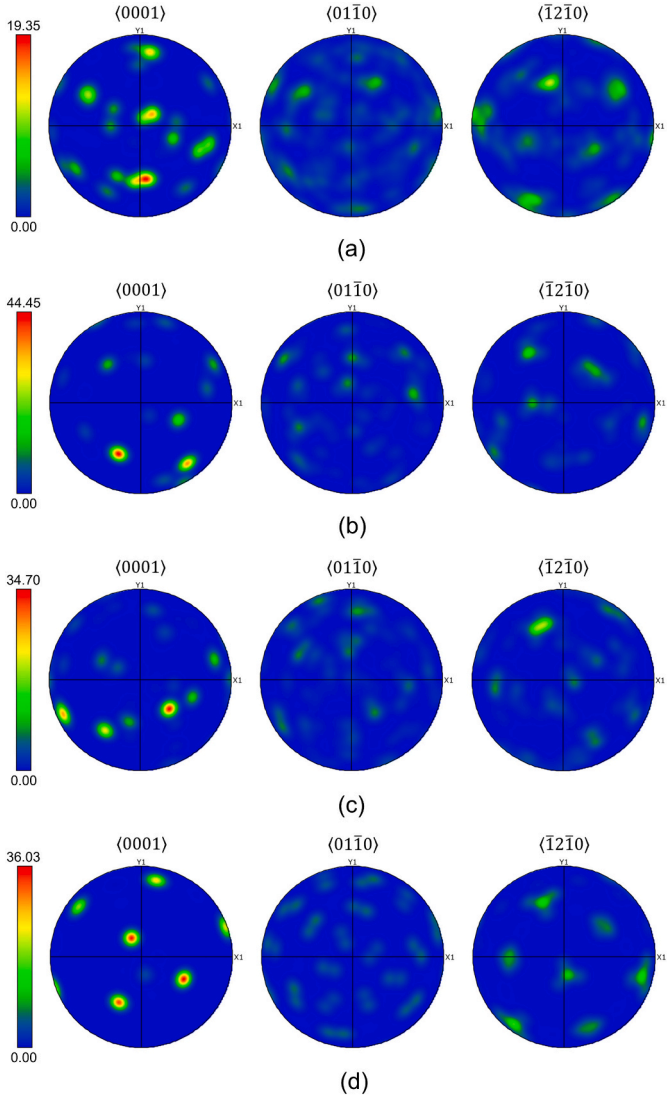

Fig. 9. PF relative to the orientation maps of the AB (a), FC (b). AC (c) and WQ (d) samples.

sum up, the higher texture found in the heat-treated samples could be related to the impossibility to consider a high number of prior-β grains simultaneously. This results from the significant grain enlargement that the samples undergo during the annealing and the variant selection mechanism that occurs when cooling from $T > T_\beta$. Furthermore, this effect is expected to be emphasized at high Z values, due to the larger prior-β grains found at higher height values (Fig. 6).

To further investigate the mechanisms governing the β → α/α' transformation from a crystallographic point of view, the distribution curves relative to the misorientation angles between neighbor laths were analyzed (Fig. 10). A main peak around 60° was detected for all the specimen and a secondary peak at 90° was also found. These results are in good agreement with the typical misorientation angles between variants [43], thus confirming that the β to α transformation governs the final texture of the material via variant selection mechanisms [39]. Moreover, a relevant tertiary peak around 10° was detected exclusively in the FC specimens. These typical misorientation curves are strictly related to the thermal history underwent by the samples. By contrast, conventional Ti-6Al-4 V (hot-rolled) is usually characterized by misorientation angles <20° [40,44].

The amount of low angle grain boundaries (LAGBs) (2°-15°) and high angle grain boundaries (HAGBs) (>15°) was also estimated by means of

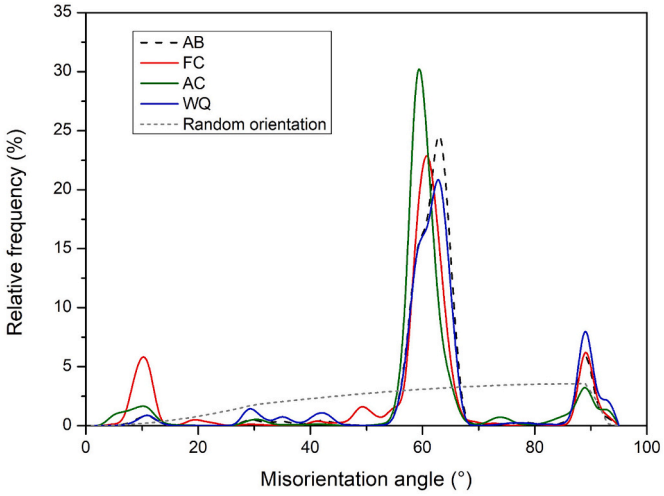

Fig. 10. Misorientation angle distribution curves relative to neighbor grain pairs, obtained by means of EBSD analyses.

EBSD. The AB and WQ samples, both characterized by a largely martensitic microstructure, provided a high fraction of HABGs ~95%. Conversely, the FC and AC specimens, characterized more stable α + β microstructures, had a lower amount of HAGBs ~80%.

The Vickers microhardness was measured on all the samples by averaging the results obtained at different heights along their cross-section. However, a clear trend along the height of the heat-treated samples was not found, suggesting that a super-β transus annealing followed by aging can be an effective mean to eliminate the intrinsic hardness anisotropy induced by the DED fabrication process in the AB samples, as determined in a previous work from the authors [20]. The average hardness values for each condition are reported in Table 4.

A slight drop in hardness was measured in the FC samples with respect to the AB ones. This decrease was related to the disappearance of α', which is a moderate hardener. The highest HV was measured in the AC specimens, even if no traces of martensite were found. The authors referred the hardness increase to the very fine microstructure that characterized these group of samples (Fig. 4a). Moreover, the high fraction of interstitial element possibly played a key role in raising the hardness, as O and N are well known hardening agents [45]. The WQ samples provided the closest mean values to the AB state, coherently with the similar microstructure that characterizes these conditions.

4. Conclusions

In this work the effect of a super β-transus annealing followed by either furnace cooling, air cooling or water quenching and then aging on DED-produced Ti-6Al-4 V samples was investigated. The gathered results allow to draw the following conclusions:

- The diverse recrystallisation heat treatments generated different types of microstructures. Namely, lamellar α + β with colonies, lamellar α + β basket-weave and martensitic α' with spare α laths, for the FC, AC and WQ specimens, respectively.

Table 4
Average microVickers values.

Condition	Average HV
AB	311 ± 27
FC	295 ± 40
AC	347 ± 25
WQ	316 ± 20

- Heat treating the DED-produced samples at $T > T_\beta$ eliminated the columnar prior-β grain morphology in favor of an equiaxed one. However, a "grain memory" effect was found resulting in increasing grain size along Z. Therefore, even if a complete microstructural recrystallisation occurred, the intrinsic grains inhomogeneity correlated to the manufacturing process remained.
- Texture analyses reported an increase in the intensity of the preferential crystallographic directions after the heat treatments. This phenomenon was probably exacerbated by the instrument magnification limit to accurately compare samples characterized by microstructural features differing by orders of magnitude in size. Notwithstanding that, a strong texture effect inside each prior-β grain was confirmed.
- The AB and WQ specimens were characterized by similar microstructural features (α') and presented similar HV values. The disappearance on the martensite in the FC samples led to a reduction in hardness. Conversely, the AC condition was comparatively harder. However, this effect was probably correlated to the significant interstitial elements pick-up that occurred during the heat treatments.

In this paper the impact of the heat treatments on the tensile properties was not assessed. Its determination is worthy of investigation in future works, since ductility improvement is a critical issue for the DED-processed Ti-6Al-4 V alloy.

Declaration of Competing Interest

The authors declare that they have no known competing financial interests or personal relationships that could have appeared to influence the work reported in this paper.

Acknowledgements

The authors would like to acknowledge the European Horizon 2020 research and innovation program; grant agreement No. 723795 / 4D Hybrid–Novel ALL-IN-ONE machines, robots and systems for affordable, worldwide and lifetime distributed 3D hybrid manufacturing and repair operations. The authors would also like to acknowledge the European Horizon 2020 research and innovation program; grant agreement No. 717194 / AMATHO (Additive MAnufacturing for Tiltrotor HOusing).

References

[1] W.E. Frazier, Metal additive manufacturing: a review, J. Mater. Eng. Perform. 23 (2014) 1917–1928, https://doi.org/10.1007/s11665-014-0958-z.
[2] S.M. Kelly, S.L. Kampe, Microstructural evolution in laser-deposited multilayer Ti-6Al-4V builds: Part II. Thermal Modeling, Metall. Mater. Trans. A Phys. Metall. Mater. Sci 35 A (2004) 1869–1879, https://doi.org/10.1007/s11661-004-0095-7.
[3] G. Lütjering, J.C. Williams, Titanium Book, 2007, https://doi.org/10.10007/978-3-540-71398-2.
[4] C. Leyens, M. Peters, Titanium and Titanium Alloys: Fundamentals and Applications, 2003.
[5] W. Hofmeister, M. Griffith, Solidification in direct metal deposition by LENS processing, JOM. 53 (2001) 30–34, https://doi.org/10.1007/s11837-001-0066-z.
[6] L. Wang, S.D. Felicelli, J.E. Craig, Experimental and numerical study of the LENS rapid fabrication process, J. Manuf. Sci. Eng. 131 (2009).
[7] B.E. Carroll, T.A. Palmer, A.M. Beese, Anisotropic tensile behavior of Ti-6Al-4V components fabricated with directed energy deposition additive manufacturing, Acta Mater. 87 (2015) 309–320, https://doi.org/10.1016/j.actamat.2014.12.054.
[8] J.N. Rousseau, A. Bois-brochu, C. Blais, E ff ect of oxygen content in new and reused powder on microstructural and mechanical properties of Ti6Al4V parts produced by directed energy deposition, Addit. Manuf. 23 (2018) 197–205, https://doi.org/10.1016/j.addma.2018.08.011.
[9] K. Zhang, X. Tian, M. Bermingham, J. Rao, Q. Jia, Y. Zhu, X. Wu, S. Cao, A. Huang, Effects of boron addition on microstructures and mechanical properties of Ti-6Al-4V manufactured by direct laser deposition, Mater. Des. 184 (2019), 108191.
[10] M. Simonelli, Y.Y. Tse, C. Tuck, On the texture formation of selective laser melted Ti-6Al-4V, Metall. Mater. Trans. A. 45 (2014) 2863–2872.
[11] J. Alcisto, A. Enriquez, H. Garcia, S. Hinkson, T. Steelman, E. Silverman, P. Valdovino, H. Gigerenzer, J. Foyos, J. Ogren, J. Dorey, K. Karg, T. Mcdonald, O. S. Es-said, Tensile Properties and Microstructures of Laser- Formed Ti-6Al-4V 20, 2011, pp. 203–212.
[12] G.P. Dinda, L. Song, J. Mazumder, Fabrication of Ti-6Al-4V scaffolds by direct metal deposition, Metall. Mater. Trans. A. 39A (2008) 2914–2922, https://doi.org/10.1007/s11661-008-9634-y.
[13] E. Dolgun, E. Zemlyakov, S. Shalnova, M. Gushchina, V. Promahov, The influence of heat treatment on the microstructure of products manufactured by direct laser deposition using titanium alloy Ti-6Al-4V, Mater. Today Proc. 30 (2020) 688–693, https://doi.org/10.1016/j.matpr.2020.01.523.
[14] G. Suprobo, A.A. Ammar, N. Park, E.R. Baek, S. Kim, Thermal decomposition of massive phase to fine lamellar α/β in Ti–6Al–4V additively manufactured alloy by directed energy deposition, Met. Mater. Int. 25 (2019) 1428–1435, https://doi.org/10.1007/s12540-019-00304-4.
[15] Y. Lu, H.B. Tang, Y.L. Fang, D. Liu, H.M. Wang, Microstructure evolution of sub-critical annealed laser deposited Ti–6Al–4V alloy, Mater. Des. 37 (2012) 56–63, https://doi.org/10.1016/j.matdes.2011.12.016.
[16] O.G. Klimova-Korsmik, G.A. Turichin, S.A. Shalnova, M.O. Gushchina, V. V. Cheverikin, Structure and properties of Ti-6Al-4V titanium alloy products obtained by direct laser deposition and subsequent heat treatment, J. Phys. Conf. Ser. 1109 (2018), 012061.
[17] A.J. Sterling, B. Torries, N. Shamsaei, S.M. Thompson, D.W. Seely, Fatigue behavior and failure mechanisms of direct laser deposited Ti-6Al-4V, Mater. Sci. Eng. A 655 (2016) 100–112, https://doi.org/10.1016/j.msea.2015.12.026.
[18] F. Mazzucato, A. Aversa, R. Doglione, S. Biamino, A. Valente, M. Lombardi, Influence of process parameters and deposition strategy on laser metal deposition of 316L powder, Metals (Basel). 9 (2019) 1160, https://doi.org/10.3390/met9111160.
[19] A. Carrozza, F. Mazzucato, A. Aversa, M. Lombardi, F. Bondioli, S. Biamino, A. Valente, P. Fino, Single scans of Ti - 6Al - 4V by directed energy deposition : a cost and time effective methodology to assess the proper process window, Met. Mater. Int. (2021), https://doi.org/10.1007/s12540-020-00930-3.
[20] A. Carrozza, A. Aversa, F. Mazzucato, M. Lombardi, S. Biamino, A. Valente, P. Fino, An innovative approach on directed energy deposition optimization : a study of the process environment's influence on the quality of Ti-6Al-4V samples, Appl. Sci. 10 (2020).
[21] A. International, Standard test methods for determining average grain size, Astm E112-10 (2010) 1–27, https://doi.org/10.1520/E0112-13.1.4.
[22] X. Zhao, S. Li, M. Zhang, Y. Liu, T.B. Sercombe, S. Wang, Y. Hao, R. Yang, L. E. Murr, Comparison of the microstructures and mechanical properties of Ti–6Al–4V fabricated by selective laser melting and electron beam melting, Mater. Des. 95 (2016) 21–31.
[23] F. Martina, P.A. Colegrove, S.W. Williams, J. Meyer, Microstructure of interpass rolled wire+ arc additive manufacturing Ti-6Al-4V components, Metall. Mater. Trans. A. 46 (2015) 6103–6118.
[24] B.D. Cullity, S.R. Stock, Elements of X-Ray Diffraction, Addison-Wesley Publishing, 1956.
[25] J.M. Oh, B.G. Lee, S.W. Cho, S.W. Lee, G.S. Choi, J.W. Lim, Oxygen effects on the mechanical properties and lattice strain of Ti and Ti-6Al-4V, Met. Mater. Int. 17 (2011) 733–736, https://doi.org/10.1007/s12540-011-1006-2.
[26] S. Soeda, H. Fujii, H. Okano, M. Hanaki, High Strength, High Ductility Titanium-Alloy and Process for Producing the Same, 6063211, 2000.
[27] M. Yan, W. Xu, M.S. Dargusch, H.P. Tang, M. Brandt, M. Qian, Review of effect of oxygen on room temperature ductility of titanium and titanium alloys, Powder Metall. 57 (2014) 251–257, https://doi.org/10.1179/1743290114Y.0000000108.
[28] I. Polmear, D. StJohn, J.-F. Nie, M. Qian, Light Alloys: Metallurgy of the Light Metals, Butterworth-Heinemann, 2017.
[29] H. Shao, Y. Zhao, P. Ge, W. Zeng, Influence of cooling rate and aging on the lamellar microstructure and Fractography of TC21 titanium alloy, Metallogr. Microstruct. Anal. 2 (2013) 35–41, https://doi.org/10.1007/s13632-012-0055-3.
[30] G.T. Aleixo, E.S.N. Lopes, R. Contieri, A. Cremasco, C.R.M. Afonso, R. Caram, Effects of cooling rate and Sn addition on the microstructure of Ti-Nb-Sn alloys, in, Solid State Phenom., Trans Tech Publ (2011) 190–195.
[31] M.V. Pantawane, Y.H. Ho, S.S. Joshi, N.B. Dahotre, Computational assessment of thermokinetics and associated microstructural evolution in laser powder bed fusion manufacturing of Ti6Al4V alloy, Sci. Rep. 10 (2020) 1–14, https://doi.org/10.1038/s41598-020-63281-4.
[32] K. Yang, J. Wang, L. Jia, G. Yang, H. Tang, Y. Li, Additive manufacturing of Ti-6Al-4V lattice structures with high structural integrity under large compressive deformation, J. Mater. Sci. Technol. 35 (2019) 303–308, https://doi.org/10.1016/j.jmst.2018.10.029.
[33] B. Wysocki, P. Maj, R. Sitek, J. Buhagiar, K.J. Kurzydłowski, W. Święszkowski, W. Świeszkowski, Laser and electron beam additive manufacturing methods of fabricating titanium bone implants, Appl. Sci. 7 (2017) 657, https://doi.org/10.3390/app7070657.
[34] M. Nabhani, R. Shoja Razavi, M. Barekat, Corrosion study of laser cladded Ti-6Al-4V alloy in different corrosive environments, Eng. Fail. Anal. 97 (2019) 234–241, https://doi.org/10.1016/j.engfailanal.2019.01.023.
[35] J. Cho, Characterization of the α'-Martensite Phase and its Decomposition in Ti-6Al-4V Additively Manufactured by Selective Laser Melting, RMIT University, 2018.
[36] J.C. Williams, A.F. Belov, Titanium and Titanium Alloys: Scientific and Technological Aspects, 1982.
[37] F.J. Gil, J.A. Planell, Growth order and activation energies for grain growth of Ti6Al4V alloy in ß phase, Scr. Metall. Mater. 25 (1991) 2843–2848, https://doi.org/10.1016/0956-716X(91)90167-Y.

[38] H. Yu, W. Li, H. Zou, S. Li, T. Zhai, L. Liu, Study on non-isothermal transformation of Ti-6Al-4V in solution heating stage, Metals (Basel). 9 (2019), https://doi.org/10.3390/met9090968.
[39] C.M. Cepeda-Jiménez, F. Potenza, E. Magalini, V. Luchin, A. Molinari, M.T. Pérez-Prado, Effect of energy density on the microstructure and texture evolution of Ti-6Al-4V manufactured by laser powder bed fusion, Mater. Charact. 110238 (2020).
[40] J. Dai, J. Xia, L. Chai, K.L. Murty, N. Guo, M.R. Daymond, Correlation of microstructural, textural characteristics and hardness of Ti–6Al–4V sheet β-cooled at different rates, J. Mater. Sci. 55 (2020) 8346–8362.
[41] A.A. Antonysamy, J. Meyer, P.B. Prangnell, Effect of build geometry on the β-grain structure and texture in additive manufacture of Ti6Al4V by selective electron beam melting, Mater. Charact. 84 (2013) 153–168, https://doi.org/10.1016/j.matchar.2013.07.012.
[42] C. de Formanoir, S. Michotte, O. Rigo, L. Germain, S. Godet, Electron beam melted Ti-6Al-4V: microstructure, texture and mechanical behavior of the as-built and heat-treated material, Mater. Sci. Eng. A 652 (2016) 105–119, https://doi.org/10.1016/j.msea.2015.11.052.
[43] N. Gey, M. Humbert, Characterization of the variant selection occurring during the α→ β→ α phase transformations of a cold rolled titanium sheet, Acta Mater. 50 (2002) 277–287.
[44] J.-Y. Xia, L.-J. Chai, H. Wu, Y. Zhi, Y.-N. Gou, W.-J. Huang, N. Guo, EBSD study of microstructural and textural changes of hot-rolled Ti–6Al–4V sheet after annealing at 800 C, Acta Metall. Sin. (English Lett.) 31 (2018) 1215–1223.
[45] C. Ouchi, H. Iizumi, S. Mitao, Effects of ultra-high purification and addition of interstitial elements on properties of pure titanium and titanium alloy, Mater. Sci. Eng. A 243 (1998) 186–195.